Particle-number-projected thermal pairing

Nguyen Dinh Dang*
Heavy-Ion Nuclear Physics Laboratory, Nishina Center for Accelerator-Based Science, RIKEN, 2-1 Hirosawa, Wako city, 351-0198 Saitama, Japan and
Institute for Nuclear Science and Technique, Hanoi, Vietnam
(Received 5 August 2007; revised manuscript received 1 October 2007; published 28 December 2007)

Particle-number projection is applied to the modified BCS (MBCS) theory. The resulting particle-number-projected MBCS theory, taking into account the effects due to fluctuations of particle and quasiparticle numbers at finite temperature, is tested within the exactly solvable multilevel model for pairing as well as the realistic ^{120}Sn nucleus. The signature of the pseudogap in the crossover region above the critical temperature of superfluid-normal phase transition is discussed in terms of the pairing spectral function.

DOI: 10.1103/PhysRevC.76.064320 PACS number(s): 21.60.−n, 24.10.Pa, 24.60.Ky, 27.60.+j

I. INTRODUCTION

The BCS theory and its generalization, the Hartree-Fock-Bogoliubov (HFB) theory at finite temperature, describe well the superfluid-normal (SN) phase transition from the superconducting (superfluid) state to the normal one in infinite systems. By solving the finite-temperature BCS (FT-BCS) equations for a constant level density around the chemical potential, the critical temperature T_c, at which the pairing gap for metal superconductors [1] and nuclear matter sharply vanishes, is found to be $0.567\Delta(T = 0)$ [2,3]. These theories use a simple variational ground-state wave function as a collection of coherent pairs acting on the particle vacuum. As a result, one obtains a set of nonlinear equations for the pairing gap and the chemical potential within the BCS theory, which can be easily solved, or a small-dimension matrix within the HFB theory, which can be diagonalized. Although the pairing problem can be exactly solved by various methods [4–6], the simplicity of the BCS and HFB theories still makes them a preferable choice in the study of finite systems such as atomic nuclei, whose realistic configuration space quite often prevents the feasibility of the exact solutions. However, when the BCS and HFB theories are applied to such small systems, modifications are required, since the finiteness of the systems causes large quantal and statistical (thermal) fluctuations, whose effects are ignored in these theories. These fluctuations increase with decreasing particle number N. With increasing temperature T one also witnesses a decrease of quantal fluctuations and increase of statistical ones.

Quantal fluctuations (QF) within the BCS (HFB) theory include the particle-number fluctuations. The latter exist even at zero temperature $T = 0$ because of the violation of particle number in the BCS ground-state wave function, which is not an eigenstate of the particle-number operator. To eliminate this defect of the BCS (HFB) theory, various methods of particle-number projection (PNP) have been proposed, which project out that component of the BCS wave function which corresponds to the right number of particles. These PNP methods can be classified as the projection after variation (PAV) and variation after projection (VAP) ones. In the PAV method, the BCS (HFB) wave function is used to calculate the projected energy of the system, whereas the VAP method determines the wave function by minimizing the projected energy. With respect to the BCS (HFB) theory, naturally, the VAP approach is much better than the PAV, in particular in the region where the BCS (HFB) theory breaks down, namely, at very weak interaction and/or temperature above T_c. Among the VAP methods, the one proposed by Lipkin and Nogami is quite popular because it is computationally simple albeit approximate. Within the Lipkin-Nogami (LN) method [7,8], the expectation value of the pairing Hamiltonian with respect to the projected BCS state is expressed in terms of that with respect to the unprojected BCS state. The approximation consists of truncating the infinite expansion series at the second order of the particle-number operator N. As a result, one ends up with minimizing the Hamiltonian $H - \lambda_1 N - \lambda_2 N^2$. The elegance of this method is that, unlike λ_1, the expansion coefficient λ_2 is not a Lagrangian multiplier, but analytically expressed in terms of coefficients u_j and v_j of the Bogoliubov transformation from particles to quasiparticles. The LN equations for the gap and particle number, therefore, are as simple as the BCS ones. Different from the BCS theory, which has nontrivial (nonzero) solutions only above a critical value G_c of the pairing-interaction parameter G, the LN equations have nontrivial solutions at any $G \neq 0$, which are quite close to the exact ones when tested in schematic models [8–10].

Statistical fluctuations (SF) in the pairing field have been studied in several papers within the approaches based on Landau's (macroscopic) theory of phase transitions [11–13] and the static-path approximation [14]. The results of these studies show a nonvanishing pairing gap as a function of temperature in the presence of SF. The gap does not collapse at the critical temperature T_c as has been predicted by the BCS theory but decreases monotonously as the temperature increases and remains finite even at rather high T. The conclusion is that thermal fluctuations in the pairing field wash out the SN phase transition. While the conventional BCS and HFB theories at finite temperature ignore the quasiparticle-number fluctuation (QNF) [12], the recently proposed modified BCS (MBCS) theory [15–17] and its generation, the modified HFB (MHFB)

*dang@riken.jp

theory [18], have taken into account the effects due to QNF based on a microscopic foundation. This is realized through a secondary Bogoliubov transformation from quasiparticle operators to modified quasiparticle ones that allows one to include the QNF in the generalized single-particle matrix. As a result, the unitarity relation, which is violated within the conventional BCS and HFB theories at finite temperature [12], is restored. It has been shown for the first time within the MBCS theory [15–17] that it is the QNF that smoothes out the sharp SN phase transition and leads to the nonvanishing thermal pairing in finite systems. The existence (or appearance) of a pairing gap at finite temperature above the critical temperature T_c of the SN-phase transition in finite systems is quite similar to that of pairing correlations in the crossover region from a BCS-like phase-ordered band structure to a new phase-disordered pseudogapped band structure discussed recently in the BCS–Bose-Einstein condensation crossover theory for high-temperature superconductors and ultracold atomic Fermi gases [19]. As a matter of fact, the high-temperature tail of the MCBCS gap is driven mostly by the QNF.

Since the effects of QF are still neglected within the MBCS (MHFB) theory, to give a conclusive answer to the question for SN phase transition in finite systems it is necessary to carry out a PNP in combination with the MBCS (MHFB) theory. This task has been pointed out in the previous paper [17] and is the aim of the present paper, where the PNP will be carried out in two ways. In the first way, the VAP is carried out by using the LN method within the BCS theory, and then the resulting approach is modified by using the secondary Bogoliubov transformation to include the effect of QNF. In the second way, the PAV is applied to the total energy of the system obtained within the MBCS theory to extract the effective thermal gap. The reason that the PAV is reliable in this case is that it is carried out after solving the MBCS equations, which include the effect of QNF beyond the BCS theory. These two ways of combining the PNP with the MBCS theory will be referred to as the modified Lipkin-Nogami (MLN) method and the PAV-MBCS theory, respectively.

The paper is organized as follows. The particle-number-projected MBCS (PNP-MBCS) theory is discussed in Sec. I within the MLN and PAV-MBCS. The results of numerical calculations carried out for an exactly solvable model as well as for a realistic nucleus are analyzed in Sec. II. The equidistant multilevel model called the Richardson model for pairing and the neutron spectrum obtained within the Woods-Saxon potential for ^{120}Sn are used in these calculations. The last section summarizes the paper, where conclusions are drawn.

II. PNP-MBCS THEORY

A. Outline of MBCS theory

The MBCS theory and its generation, the MHFB theory, have been discussed in detail in a series of papers [15–18]. Therefore, only the outline of the MBCS theory is given in this section, which will be used for the application of the PNP in the next section.

The MBCS theory includes the QNF by using the following secondary Bogoliubov transformation from quasiparticle operators, $\alpha^\dagger_{jm}$ and α_{jm}, to the modified quasiparticle ones, $\bar\alpha^\dagger_{jm}$ and $\bar\alpha_{jm}$, that is,

$$\begin{aligned}\bar\alpha^\dagger_{jm} &= \sqrt{1-n_j}\,\alpha^\dagger_{jm} + \sqrt{n_j}\,\alpha_{j\tilde m},\\ \bar\alpha_{j\tilde m} &= \sqrt{1-n_j}\,\alpha_{j\tilde m} - \sqrt{n_j}\,\alpha^\dagger_{jm},\end{aligned} \tag{1}$$

where the indices j and m denote the angular-momentum quantum numbers of single-particle orbitals, while the sign $\tilde{}$ stands for the time-reversal operation, e.g., $a_{j\tilde m} = -\mathcal{T}a_{j-m} \equiv (-)^{j-m}a_{j-m}$, and n_j is the quasiparticle occupation number. By applying successively the original Bogoliubov transformation from particle operators to quasiparticle ones and the transformation (1), one obtains the combined transformation between particle and modified quasiparticle operators as

$$a^\dagger_{jm} = \bar u_j\bar\alpha^\dagger_{jm} + \bar v_j\bar\alpha_{j\tilde m}, \qquad a_{j\tilde m} = \bar u_j\bar\alpha_{j\tilde m} - \bar v_j\bar\alpha^\dagger_{jm}, \tag{2}$$

The coefficients $\bar u_i$ and $\bar v_i$ of the combined transformation (2) are given as

$$\bar u_j = u_j\sqrt{1-n_j} + v_j\sqrt{n_j}, \qquad \bar v_j = v_j\sqrt{1-n_j} - u_j\sqrt{n_j}. \tag{3}$$

By applying the transformation (2), one rewrites the pairing Hamiltonian

$$H = \sum_{jm}\epsilon_j a^\dagger_{jm}a_{jm} - \frac{1}{4}G\sum_{jj'mm'} a^\dagger_{jm}a^\dagger_{j\tilde m}a_{j'\tilde m'}a_{j'm'} \tag{4}$$

in the modified-quasiparticle representation. Because of the formal Eq. (2), the result has the same form as that of the quasiparticle representation for H, but with the modified-quasiparticle operators $\bar\alpha^\dagger_i$, $\bar\alpha_i$ replacing the quasiparticle ones $\alpha^\dagger_i$, α_i, and coefficients $\bar u_i$, $\bar v_i$ replacing u_i, v_i [see Eqs. (7)–(13) of Ref. [16]]. The rest of the derivation followed the same way as that for the BCS equation. The final result yields the MBCS equation in the form [17]

$$\bar\Delta = G\sum_j \Omega_j\bar\tau_j, \qquad N = 2\sum_j\Omega_j\bar\rho_i, \tag{5}$$

where the modified single-particle density matrix $\bar\rho_j$ and modified particle-pairing tensor $\bar\tau_j$ are different from the conventional temperature-dependent single-particle density matrix ρ_j and particle-pairing tensor τ_j by the terms containing the QNF on j-th orbitals, $\delta\mathcal{N}_j$, namely,

$$\bar\rho_j = \rho_j - 2u_jv_j\delta\mathcal{N}_j, \qquad \bar\tau_j = \tau_j - \left(u_j^2 - v_j^2\right)\delta\mathcal{N}_j, \tag{6}$$

with

$$\begin{aligned}\rho_j &= v_j^2 + \left(1-2v_j^2\right)n_j,\\ \tau_j &= u_jv_j(1-2n_j),\\ \delta\mathcal{N}_j &= \sqrt{n_j(1-n_j)},\end{aligned} \tag{7}$$

and the shell degeneracy $2\Omega_j \equiv 2j+1$. The quasiparticle occupation number n_j is defined within the MBCS theory by the Fermi-Dirac distribution of free quasiparticles, that is,

$$n_j = \frac{1}{e^{\bar E_j/T}+1}, \tag{8}$$

where $\bar{E}_j$ is the modified quasiparticle energy

$$\bar{E}_j = \sqrt{(\epsilon'_j - \lambda)^2 + \bar{\Delta}^2}, \tag{9}$$

with $\epsilon'_j = \epsilon_j - Gv_j^2$, including the self-energy term $-Gv_j^2$, or $\epsilon'_j = \epsilon_j$ if the self-energy term is neglected. The MBCS internal energy is given by an expression similar to that of the BCS one as follows:

$$\mathcal{E}_{\rm MBCS} = \sum_j \Omega_j \left[2\epsilon_j \bar{v}_j^2 - G\bar{v}_j^4\right] - \frac{\bar{\Delta}^2}{G}. \tag{10}$$

Neglecting the term $\sim -G\bar{v}_j^4$, one recovers from Eq. (10) the expression for the MBCS energy used in Refs. [16–18]. In the present paper, the complete expression (10) will be used.

The gap and number equations (5) clearly show how the QNF is included within the MBCS theory. This leads to the appearance of the thermal component $\delta\Delta$ in the pairing gap $\bar{\Delta}$,

$$\delta\Delta = -G\sum_j \Omega_j \left(u_j^2 - v_j^2\right)\delta\mathcal{N}_j, \tag{11}$$

in addition to the quantal one, $\Delta = G\sum_j \Omega_j \tau_j$, so that $\bar{\Delta} = \Delta + \delta\Delta$. The thermal component $\delta\Delta$ is generated only by QNF. As the temperature decreases, the quasiparticle occupation number n_j decreases. As a result, $\delta\Delta$ gets depleted while Δ becomes enhanced. This behavior closely recalls the thermal precursor superconducting fluctuations, which cause the incoherent preformed pairs leading to gaplike features (pseudogap) observed at $T > T_c$ in high-temperature superconductors [19]. As T decreases, thermal fluctuations (of the phase) are suppressed to a point at which the pairs becomes sufficiently coherent to cause superconductivity. Therefore, in the rest of the paper, the thermal component $\delta\Delta$ of the MBCS gap $\bar{\Delta}$ will be called the pseudogap, keeping in mind that the connection between the QNF and classical phase fluctuations at $T \neq 0$ deserves a thorough study.

B. Modified Lipkin-Nogami method

The MLN method consists of two self-consistent steps. In the first step, the LN method is applied to remove the particle-number fluctuations inherent in the BCS theory. This leads to a renormalization of the single-particle and quasiparticle energies as

$$\widetilde{\epsilon}_j = \epsilon_j + (4\lambda_2 - G)v_j^2, \quad \widetilde{E}_j = \sqrt{(\widetilde{\epsilon}_j - \lambda)^2 + \bar{\Delta}^2}, \tag{12}$$

where

$$\lambda = \lambda_1 + 2\lambda_2(N+1), \quad v_j^2 = \frac{1}{2}\left[1 - \frac{\widetilde{\epsilon}_j - \lambda}{\widetilde{E}_j}\right], \quad u_j^2 = 1 - v_j^2. \tag{13}$$

In the next step, one determines the modified pairing gap $\bar{\Delta}$ and λ from the same MBCS equations (5), where coefficients u_j and v_j from Eq. (13) are used to determine $\bar{u}_j$ and $\bar{v}_j$ in Eq. (3). The coefficient λ_2 has the form [20]

$$\lambda_2 = \frac{G}{4}\frac{\sum_j \Omega_j(1-\bar{\rho}_j)\bar{\tau}_j \sum_{j'} \Omega_{j'}\bar{\rho}_{j'}\bar{\tau}_{j'} - \sum_j \Omega_j(1-\bar{\rho}_j)^2\bar{\rho}_j^2}{\left[\sum_j \Omega_j\bar{\rho}_j(1-\bar{\rho}_j)\right]^2 - \sum_j \Omega_j(1-\bar{\rho}_j)^2\bar{\rho}_j^2}, \tag{14}$$

which becomes the expression for $T = 0$ given in the original paper [8] of the LN method when $n_j = 0$. The set of Eqs. (3), (12), (13), and (14) is solved self-consistently and forms the MLN equations. The total energy is given as

$$\mathcal{E}_{\rm MLN} = \sum_j \Omega_j[\epsilon_j - G\bar{\rho}_j]\bar{\rho}_j - \frac{\bar{\Delta}^2}{G} - \lambda_2 \Delta N^2, \tag{15}$$

where the particle-number fluctuation ΔN^2 is calculated as

$$\Delta N^2 = 4\sum_j \Omega_j(\bar{u}_j\bar{v}_j)^2. \tag{16}$$

By setting $\lambda_2 = 0$, one recovers the MBCS equations from the MLN ones.

C. PAV-MBCS theory

The PNP energy is realized by applying the PNP operator

$$P^N = \frac{1}{2\pi}\int d\phi e^{-i\phi(\hat{N}-N)} \tag{17}$$

to a model Hamiltonian whose expectation (average) value in the ground-state (grand canonical ensemble) corresponds to the energy under consideration. Defining the average value of an operator $\mathcal{O}$ with respect to the density operator D as

$$\langle\mathcal{O}\rangle = Tr[\mathcal{O}D], \tag{18}$$

one obtains the formal expression of the PNP pairing energy at finite temperature T as

$$\mathcal{E}^{\rm N}_{\rm pair} = \frac{\langle H_{\rm pair}P^N\rangle}{\langle P^N\rangle} = \int d\phi y^N(\phi) H_{\rm pair}(\phi), \tag{19}$$

where

$$y^N(\phi) = \frac{e^{-i\phi N}\langle e^{i\phi\hat{N}}\rangle}{\int d\phi\, e^{-i\phi N}\langle e^{i\phi\hat{N}}\rangle}, \quad H_{\rm pair}(\phi) = \frac{\langle H_{\rm pair}\, e^{i\phi\hat{N}}\rangle}{\langle e^{i\phi\hat{N}}\rangle}. \tag{20}$$

The thermal average $\langle e^{i\phi\hat{N}}\rangle$ is determined in terms of the generalized particle-density matrix R as

$$\langle e^{i\phi\hat{N}}\rangle = \det\sqrt{e^{i\phi/2}\mathcal{C}(\phi)}, \quad \mathcal{C}(\phi) = 1 + (e^{i\phi N} - 1)R, \tag{21}$$

with R given by Eq. (17) of Ref. [18]. Within the HFB theory, the idempotent $R^2 = R$ no longer holds at $T \neq 0$, and the difference is just the QNF, namely, $R^2(T) - R(T) = \sum_j \Omega_j \delta\mathcal{N}_j$ [12,21]. A merit of the MHFB theory is that it restores the idempotent $\bar{R}^2(T) = \bar{R}(T)$ for the modified generalized particle-density matrix $\bar{R}$ defined by Eq. (40) of Ref. [18]. As a result, the modified matrix $\bar{C}(\phi)$ becomes

$$\bar{\mathcal{C}}(\phi) = \frac{e^{2i\phi}}{\bar{D}(\phi)}, \quad \bar{D}(\phi) = 1 + \bar{\rho}(e^{2i\phi} - 1), \tag{22}$$

i.e., it acquires the same form as that obtained at $T = 0$. All the temperature dependence is now included in the u_j, v_j coefficients and in the QNF $\delta\mathcal{N}_j$ of the modified single-particle density $\bar{\rho}_j$.

By using Eqs. (20) and (22) as well as $H_{\rm pair} = -GP^\dagger P$, which is given in the spherical basis as the last term at the right-hand side of Hamiltonian (4), one obtains the PNP pairing energy as

$$\mathcal{E}^{\rm N}_{\rm pair} = -G\frac{\int d\phi\, e^{-i\phi N}\{[\sum_j \Omega_j \bar{u}_j\bar{v}_j\bar{D}_j(\phi)^{-1}]^2 + \sum_j \Omega_j \bar{v}_j^4 \bar{D}_j(\phi)^{-1}\}e^{i\phi}[\prod_{j'}\bar{D}_{j'}(\phi)]^{1/2}}{\int d\phi e^{-i\phi N}[\prod_{j'}\bar{D}_{j'}(\phi)]^{1/2}}. \quad (23)$$

For comparison with the pairing gaps determined within the MBCS theory and MLN method, it is convenient to define an effective gap from the PNP pairing energy as

$$\Delta_{\rm PNP} = \sqrt{-G\mathcal{E}^N_{\rm pair}}. \quad (24)$$

It is worth noticing that the term $-G\sum_j \Omega_j \bar{v}_j^4$ is included in the definition of the effective gap $\Delta_{\rm PNP}$.

D. Probing the presence of a pseudogap by using thermodynamic quantities

1. Heat capacity

A clear signature of the SN (second-order) phase transition is the disconvergence of the heat capacity C at the critical temperature $T = T_c$. The heat capacity C is defined as

$$C(T) = \frac{\partial \mathcal{E}}{\partial T}, \quad (25)$$

where $\mathcal{E}$ is the total (internal) energy of the system. As has been shown in Refs. [17,18], the nonvanishing MBCS pairing gap due to the effect of QNF leads to the smoothing of the sharp disconvergence in the heat capacity C calculated within MBCS theory. Therefore C can be used to examine the presence of the pseudogap $\delta\Delta$ in Eq. (11).

2. Entropies

A quantity that is directly related to the heat capacity is the thermodynamic entropy $S_{\rm th}$, which is defined from the condition of thermal equilibrium of a closed system, that is,

$$\frac{\partial S_{\rm th}}{\partial \mathcal{E}} = \frac{1}{T}. \quad (26)$$

Integrating Eq. (26), one obtains the thermodynamic entropy $S_{\rm th}$ in the form

$$S_{\rm th} = \int_0^T \frac{1}{\tau}\frac{\partial \mathcal{E}}{\partial \tau}d\tau = \int_0^T \frac{1}{\tau}C(\tau)\,d\tau. \quad (27)$$

In general, the thermodynamic entropy $S_{\rm th}$ is different from the quasiparticle or single-particle entropy as the latter corresponds to the purely mean-field picture. The quasiparticle entropy within the MBCS theory has the same form as that obtained within the conventional BCS theory [17,18]:

$$S_{\rm qp} = -2\sum_j \Omega_j[n_j \ln n_j + (1-n_j)\ln(1-n_j)]. \quad (28)$$

The relationship between the thermodynamic, single-particle, and information entropies were studied in Ref. [22], which shows that the thermodynamic and single-particle entropies are nearly the same only for noninteracting particles. For the realistic mean fields with empirical residual interactions, these entropies are different at the edges of their distributions over single-particle levels. This leads to the difference between the low thermodynamic temperature and single-particle temperature, which are extracted by using $S_{\rm th}$ and $S_{\rm qp}$, respectively.

3. Pairing spectral function

Another quantity used to probe the presence of a pseudogap is the pairing spectral function $I_j(\omega)$, which is derived from the modified quasiparticle Green's function $\bar{G}_j(E)$ [3]

$$\bar{G}_j(E) = \frac{1}{2\pi}\left[\frac{\bar{u}_j^2}{E-\bar{E}_j} + \frac{\bar{v}_j^2}{E+\bar{E}_j}\right] \quad (29)$$

as follows. Using the analytic property of Green's function $\bar{G}_j(E)$ to continue it into the complex energy plane $E = \omega + i\varepsilon$ (ω and ε are real) and taking the imaginary part of this analytic continuation, one finds the quasiparticle spectral function $\mathcal{J}_j(\omega)$ in the form

$$\mathcal{J}_j(\omega) = \frac{1}{\pi}\left[\frac{\bar{u}_j^2\varepsilon}{(\omega-\bar{E}_j)^2+\varepsilon^2} + \frac{\bar{v}_j^2\varepsilon}{(\omega+\bar{E}_j)^2+\varepsilon^2}\right]. \quad (30)$$

The two-quasiparticle spectral function $I_{jj'}(\omega)$ is derived in the same way as the imaginary part of the analytic continuation of the two-quasiparticle Green's function. The latter is obtained by folding two Green's functions $G_j(E)$ and $G_{j'}(E)$. The final result reads

$$\begin{aligned} I_{jj'}(\omega) = \frac{2}{\pi}\Bigg[&\frac{\bar{u}_j^2\bar{u}_{j'}^2\varepsilon}{(\omega-\bar{E}_j-\bar{E}_{j'})^2+4\varepsilon^2} \\ &+ \frac{\bar{v}_j^2\bar{v}_{j'}^2\varepsilon}{(\omega+\bar{E}_j+\bar{E}_{j'})^2+4\varepsilon^2} \\ &+ \frac{\bar{u}_j^2\bar{v}_{j'}^2\varepsilon}{(\omega-\bar{E}_j+\bar{E}_{j'})^2+4\varepsilon^2} \\ &+ \frac{\bar{v}_j^2\bar{u}_{j'}^2\varepsilon}{(\omega+\bar{E}_j-\bar{E}_{j'})^2+4\varepsilon^2}\Bigg]. \end{aligned} \quad (31)$$

The pairing spectral function $I_j(\omega)$ is obtained by setting $j = j'$ in Eq. (31). As a result, one obtains

$$I_j(\omega) = \frac{2}{\pi}\left[\frac{\bar{u}_j^4\varepsilon}{(\omega - 2\bar{E}_j)^2 + 4\varepsilon^4} + \frac{\bar{v}_j^4\varepsilon}{(\omega + 2\bar{E}_j)^2 + 4\varepsilon^2} + \frac{2\bar{u}_j^2\bar{v}_j^2\varepsilon}{\omega^2 + 4\varepsilon^2}\right]. \quad (32)$$

The calculation of the pairing spectral function $I_j(\omega)$ includes the parameter ε equal to the half-width of the pairing excitation, whose lifetime is $1/(2\varepsilon)$. At $T = 0$, the quasiparticle occupation numbers n_j vanish so the coefficients $\bar{u}_j$ and $\bar{v}_j$ in Eq. (3) become the conventional Bogoliubov coefficients u_j and v_j, and the expression for the BCS case is recovered from Eq. (32). The total pairing spectral function $J(\omega)$ is calculated from Eq. (32) as

$$J(\omega) \equiv \sum_j I_j(\omega) = J_U(\omega) + J_V(\omega) + J_{UV}(\omega), \quad (33)$$

where

$$J_U(\omega) = \frac{2}{\pi}\sum_j \frac{\bar{u}_j^4\varepsilon}{(\omega - 2\bar{E}_j)^2 + 4\varepsilon^4}, \quad (34)$$

$$J_V(\omega) = \frac{2}{\pi}\sum_j \frac{\bar{v}_j^4\varepsilon}{(\omega + 2\bar{E}_j)^2 + 4\varepsilon^2},$$

$$J_{UV}(\omega) = \frac{4}{\pi}\sum_j \frac{\bar{u}_j^2\bar{v}_j^2\varepsilon}{\omega^2 + 4\varepsilon^2}. \quad (35)$$

Using the total pairing spectral function $J(\omega)$, one can also calculate the k-th moment m_k, the energy centroid $\bar{E}$, and the deviation σ from the energy centroid as follows:

$$m_k = \int_{E_1}^{E_2} \omega^k J(\omega) d\omega, \qquad \bar{E} = \frac{m_1}{m_0}, \qquad \sigma = \sqrt{\frac{m_2}{m_0} - \bar{E}^2}. \quad (36)$$

The zeroth and first moments are also called the total and energy-weighted sums of strengths, respectively, while the deviation σ is also referred to as the spreading width.

III. NUMERICAL ANALYSIS

The calculations were carried out within the Richardson model[1] and for ^{120}Sn. The Richardson model consists of Ω doubly folded equidistant levels, which interact via a pairing force with a constant parameter G. The single-particle energies take the values $\epsilon_j = j\epsilon$ with the index j running over all Ω levels. The model is called half-filled when the number Ω of levels is equal to the number N of particles. This particle-hole (p-h) symmetric case means that in the absence of interaction ($G = 0$), the lowest $\Omega_h = \Omega/2$ hole levels are occupied with $N = \Omega$ particles (two particles on each level), while the upper $\Omega_p = \Omega/2$ particle levels are empty. In general, the number of hole levels Ω_h need not be the same as the number of particle levels Ω_p, i.e., $\Omega \neq N$. The level distance $\epsilon = 1$ MeV will be used in the present paper. This model is often used to test the validity of approximated approaches to the pairing problem, as its exact solutions can be found using a number of different methods, including the Richardson method [4], the method using infinite-dimensional algebras [5], and a direct diagonalization of the pairing Hamiltonian [6]. To extend the exact eigenvalues of the Richardson model to finite temperature, one needs to average them over a statistical ensemble. As the number N of particles in the system is fixed, the preferable choice is the canonical ensemble, which does not allow the particle-number fluctuations but can share the total energy $\mathcal{E}(T)$ among its possible thermodynamic states distributed by a partition function [17].

A. Sensitivity of MBCS theory to small configuration space

The extension of exact solutions of the Richardson model to finite temperature by averaging over a statistical ensemble should be taken with some care. First of all, one should keep in mind that the exact solutions of a system with pure pairing such as those of the Richardson model do not represent a full thermalization. The seniority conservation prevents a number of particles to interact with each other. As a result, for the exact solutions, the temperatures defined in different ways do not agree [22]. Furthermore, for large N, e.g., $N > 14$, the exact solutions weighed up to high temperature are impracticable. At the same time, for small N, the small configuration space for the p-h symmetric cases ($\Omega = N$) significantly reduces the limiting temperature up to which the MBCS theory can be applied.

Such sensitivity of the MBCS prediction to a small configuration space has been the subject of persistent criticism by the authors of Ref. [23], who carried out the MBCS calculations within the Richardson model for the case with $\Omega = N = 10$ and found that the MBCS gap abruptly increases at $T \geqslant 1.75$ MeV for $G = 0.4$ MeV. In Ref. [24], we pointed out that the reason for such behavior comes from the QNF profile as a function of single-particle energies. When $\Omega = N$ is small, this profile easily becomes asymmetric with respect to the Fermi level at a rather low temperature. The asymmetry of the QNF profile increases the imbalance between the positive-definite and negative-definite parts in the sum (11) that forms the pseudogap $\delta\Delta$. When this imbalance is large, the absolute value $|\delta\Delta|$ may become larger than the quantal gap Δ. As the result, the total gap $\bar{\Delta}$ may increase, decrease, or even become negative as T increases. This issue has been discussed in detail in Refs. [17,18,24], where it has been demonstrated that for $N \leqslant 14$, it is sufficient to enlarge the space by one more level, $\Omega = N + 1$, to restore the symmetry of the QNF profile up to high temperatures [17].

The sensitivity of the QNF profile to the size of the configuration space is demonstrated in the upper panels of Fig. 1, which shows the results for QNF obtained within the MBCS theory for $N = 10$ and $\Omega = N, N + 1$, and $N + 2$ by using the pairing parameter $G = 0.4$ MeV at several temperatures. When $\Omega = 11$, the symmetry of the QNF

[1] It is also called the picket-fence model, ladder model, doubly-folded equidistant pairing model and was solved exactly for the first time by Richardson in the 1960s [4].

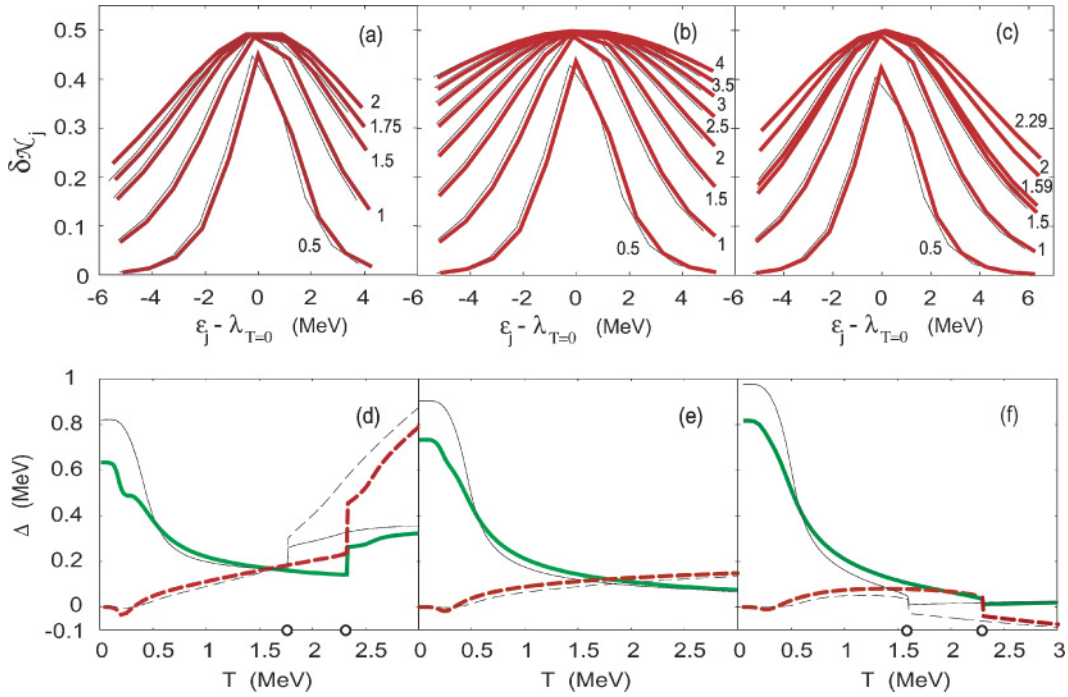

FIG. 1. (Color online) QNF profiles $\delta\mathcal{N}_j$ [(a)–(c)] at several values of T shown by the numbers at the lines, and pairing gaps [(d)–(f)] as functions of T obtained within the Richardson model for $N = 10$ and $\Omega = 10$ [(a) and (d)], $\Omega = 11$ [(b) and (e)], and $\Omega = 12$ [(c) and (f)] ($G = 0.4$ MeV). In (a)–(c), lines are used to connect discrete points to guide the eye. The thin and thick lines denote the MBCS results obtained without and including the self-energy term $-Gv_j^2$ in the single-particle energies. In (d)–(f), the solid and dashed lines denote the quantal gap Δ and the pseudogap $\delta\Delta$ [Eq. (11)], respectively, whereas the open circles on the abscissa in (d) and (f) mark the temperatures at which the gap abruptly increases (d) or decreases (f).

profiles is preserved up to rather high temperature $T >$ 5 MeV [see Fig. 1(b), which shows the QNF profiles up to $T =$ 4 MeV]. Adding or removing levels easily destroys the balance between the positive-definite and negative-definite parts in the sum (11) for the pseudogap. As a result, the symmetry of the QNF is deteriorated at a much lower value of T_M, which is about 1.75 MeV for $\Omega = 10$, and 1.6 MeV for $\Omega = 12$ if the self-energy term $-Gv_j^2$ is not taken into account in the single-particle energies [thin lines in Figs. 1(a) and 1(c)]. Adding or removing more levels, such as $\Omega = 8$ or 14, as has been tried in Ref. [25], just worsens the situation, as this further increases the imbalance and creates the asymmetry at low T_M in either direction, as shown in Figs. 1(a) or 1(c). On the other hand, a renormalization of the single-particle energies due to the residual interaction, correlations beyond the quasiparticle mean field, and/or a compression of the single-particle spectrum such as that obtained within the temperature-dependent HF calculations at high temperature [26] can also greatly enlarge the temperature region in which the MBCS theory can be applied. As demonstrated by the thick lines in Figs. 1(a) and (c), including the self-energy term in the single-particle energies significantly increases the limiting temperature up to $T_M \simeq 2.3$ MeV. This example clearly shows how the MBCS prediction depends on the single-particle spectrum. The renormalization of single-particle spectra due to correlations within the self-consistent quasiparticle random-phase approximation (SCQRPA) and its effect on the thermal pairing gap have not yet been implemented in the MBCS calculations and are subjects for further studies. This may further enlarge the temperature region in which the MBCS theory can be applied. The thorough test conducted in Ref. [17] shows that T_M for $\Omega = N$ increases linearly with the number of particles. At $N > 20$, one obtains $T_M > 5$ MeV.

Within the temperature region of its validity, the MBCS theory predicts a monotonously decreasing pairing gap with increasing T as shown in Figs. 1(d)–1(f). The figures also show that as the particle number is small ($N = 10$), the effect of the self-energy term $-Gv_j^2$ in the single-particle energies is rather strong, but it effects only the quantal gap, leaving the pseudogap almost intact. Moreover, the temperature to which the MBCS theory is valid is extended significantly to $T \simeq$ 2.3 MeV for the cases with $\Omega = 10$ and 12 as has been mentioned above. By recalling the value of the maximum temperature of around the shell distance ($\sim$ 6–8 MeV) for the large single-particle levels in realistic nuclei, one can see that for a spectrum with only 10 or 12 levels and the level distance ε of 1 MeV, a value of 2.3 MeV for the temperature is a relatively high one, to which the zero-temperature single-particle energies can be extrapolated. For realistic nuclei, the MBCS theory predicts a smoothly decreasing pairing gap up to a temperature as high as $T = 5$ MeV when a large realistic single-particle spectra such as those obtained within the Woods-Saxon potential are used [17,18].

In the present paper, to show the stability of the results of the PNP treatment, the predictions within the PNP-MBCS approaches for the pairing gaps will be compared with the exact solutions for the cases with $N = 10$ and $\Omega =$ N, $N + 1$, and $N + 2$ obtained by using the pairing parameter

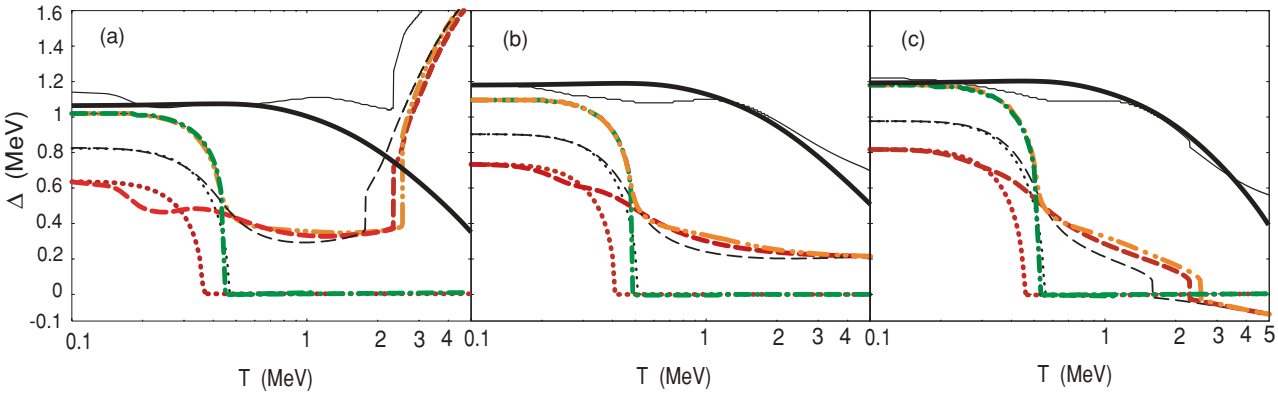

FIG. 2. (Color online) Pairing gaps as functions of temperature obtained within the Richardson model for $N = 10$ with $\Omega = N$ (a), $N + 1$ (b), and $N + 2$ (c). The BCS solutions obtained without and including the self-energy term $-Gv_j^2$ in the single-particle energies are shown with the thin and thick dotted lines, respectively. The corresponding MBCS solutions are shown by the thin and thick dashed lines, respectively. The results obtained within the LN and MLN methods are denoted by the dot-dashed and double-dot-dashed lines, respectively. The thin solid line shows the PAV-MBCS effective gap $\Delta_{\rm PNP}$, while the thick solid lines stand for the exact result.

$G = 0.4$ MeV. The predictions for thermodynamic quantities such as energies, heat capacities, and entropies will be shown for the case with $\Omega = N + 1 = 11$, for which the MBCS theory has a larger temperature region of validity (up to $T \geqslant 5$ MeV). As for the realistic nucleus ^{120}Sn, as it is a nucleus with an open neutron shell, the calculations are carried out only for neutrons by using the single-particle energies obtained within the Woods-Saxon potential and $G_\nu = 0.13$ MeV as in Ref. [18].

B. Pairing gap

The pairing gaps for $\Omega = N$, $N + 1$, and $N + 2$ are plotted in Fig. 2 as functions of T. In the region $T \leqslant T_c$, the BCS and MBCS gaps obtained including the self-energy term $-Gv_j^2$ are significantly smaller than the values predicted by the BCS and MBCS theories when this term is omitted (cf. Fig. 1). The inclusion of the self-energy term also reduces the value of T_c within the BCS theory. At $T \geqslant 0.7$ MeV, the MBCS gap obtained including the self-energy term becomes slightly larger than that obtained ignoring this term. The PNP applied by using the LN method increases the gap at $T = 0$ by nearly 47%, 40%, and 30% for $\Omega = 10$, 11, and 12, respectively. The value of T_c also rises closer to that obtained within the BCS theory ignoring the self-energy term. However, at $T > T_c$ the predictions by the MBCS theory that includes the self-energy term and by the MLN method are nearly the same, just demonstrating that the quantal fluctuations due to particle-number violation vanish at high temperature. It is also seen that in this region both of these approaches significantly underestimate the exact result. The situation is largely improved within the PAV-MBCS theory. For all Ω within the temperature region where the MBCS theory is valid, the values of the pairing gap predicted by the PAV-MBCS theory agree fairly well with the exact ones. The best example is seen in the case with $\Omega = 11$, where the PAV-MBCS prediction almost coincides with the exact results at $1 \leqslant T \leqslant 2$ MeV. At $0.2 \leqslant T \leqslant 1$ MeV, the PAV-MBCS prediction is slightly lower than the exact result; while at $T > 2$ MeV, the PAV-MBCS overestimates the exact result, and this discrepancy increases with T. For $\Omega = 12$, despite a small kink at $T \simeq 2.3$ MeV due to the size effect discussed in the preceding section, the agreement between the PAV-MBCS and exact results is still quite satisfactory. In the rest of the paper, only results for the case with $\Omega = N + 1$ will be considered.

The effect of PNP at low T becomes much weaker in the realistic nucleus ^{120}Sn, where the contribution of the self-energy term is negligible because of the large number of particles (Fig. 3). The results offered by the MBCS theory and the MLN method are close to each other even at low T, while at high T they coalesce. The increasing discrepancy between the PAV-MBCS and MBCS results with increasing T is mainly caused by the $-G\sum_j \Omega_j \bar{v}_j^4$ term, which enters in the definition of the effective gap $G_{\rm PNP}$.

C. Total and excitation energies

The total energies obtained within the approaches under consideration applied to the Richardson model are plotted as functions of T in Fig. 4(a). For ^{120}Sn, as the absolute value

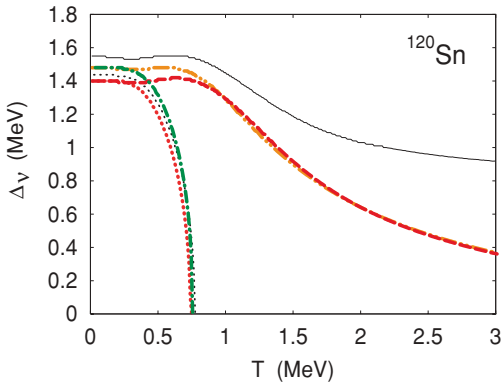

FIG. 3. (Color online) Pairing gaps as functions of temperature for neutrons in ^{120}Sn. Notations are as in Fig. 2.

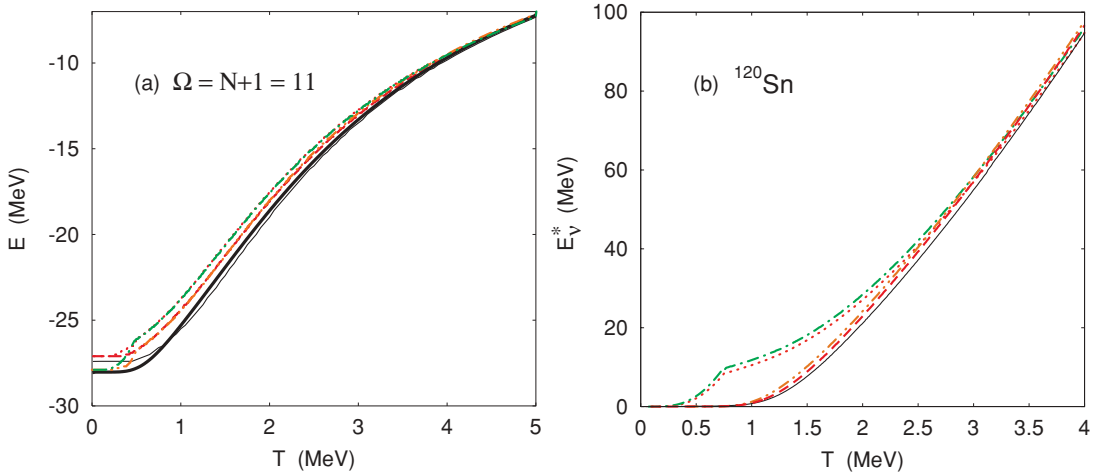

FIG. 4. (Color online) Total energy (a) and excitation energy (b) as functions of temperature obtained within the Richardson model for ($\Omega = 11$, $N = 10$) (a), and for neutrons in ^{120}Sn (b). Notations are as in Fig. 2.

of the total energy at $T = 0$ is large, the excitation energies $E^*_\nu = \mathcal{E}(T) - \mathcal{E}(0)$ for neutrons are plotted in Fig. 4(b). It is seen from this figure that the QNF indeed smoothes out the signature of the sharp SN phase transition from the total and excitation energies even after PNP is taken into account. The effect of PNP on the energies is noticeable only at very low temperature and improves greatly the agreement with the exact result [Fig. 4(a)]. Increasing the particle number reduces the difference between the predictions within MBCS, MLN, and PAV-MBCS theories. This difference becomes negligible in such realistic and heavy nuclei as ^{120}Sn [Fig. 4(b)]. At high T, all approaches predict nearly the same energy.

D. Heat capacity

The heat capacities, which are shown in Fig. 5 as functions of T, demonstrate the difference between effects caused by PNP within the MLN method and the PAV-MBCS theory. Although the gap does not collapse at T_c in both (light and heavy) systems, the effect of PNP within the MLN method is much stronger in the light system at $T < T_c$, so the slope in the pairing gap in the region around T_c is much deeper in the system with $N = 10$ than that obtained in ^{120}Sn (cf. Figs. 2 and 3). As a result, although the heat capacity in the system with $N = 10$ does not diverge within the MLN method, it still has a quite pronounced peak at $T \sim T_c$, which is completely smeared out in the case of ^{120}Sn. The PAV-MBCS theory, on the contrary, predicts a smooth temperature dependence of the heat capacity in both light and heavy systems in a much better fit to the exact result (for $N = 10$).

E. Entropies

The quasiparticle and thermodynamic entropies, $S_{\rm qp}$ and $S_{\rm th}$, obtained for ($\Omega = 11$, $N = 10$) within the Richardson model and for neutrons in ^{120}Sn are shown in Figs. 6 and 7, respectively. The clear difference between the single-particle entropy, $S_{\rm sp}$, and thermodynamic one, $S_{\rm th}$, is seen already in the exact results of the Richardson model. As the values of single-particle occupation numbers in the exact solutions obtained at $T = 0$, namely, $f_h < 1$ and $f_p > 0$, are already different from the HF ones ($f_h^{\rm HF} = 1$, $f_p^{\rm HF} = 0$), i.e., the exact $S_{\rm sp}$ does not vanish at $T = 0$. On the contrary, the thermodynamic entropy $S_{\rm th}$ always starts from zero at $T = 0$. The exact values for both $S_{\rm sp}$ and $S_{\rm th}$ increase smoothly with T, but $S_{\rm th}$ is always smaller than $S_{\rm sp}$. This observation agrees with the results in Ref. [22], which show that within the realistic mean field, the single-particle and thermodynamic entropies

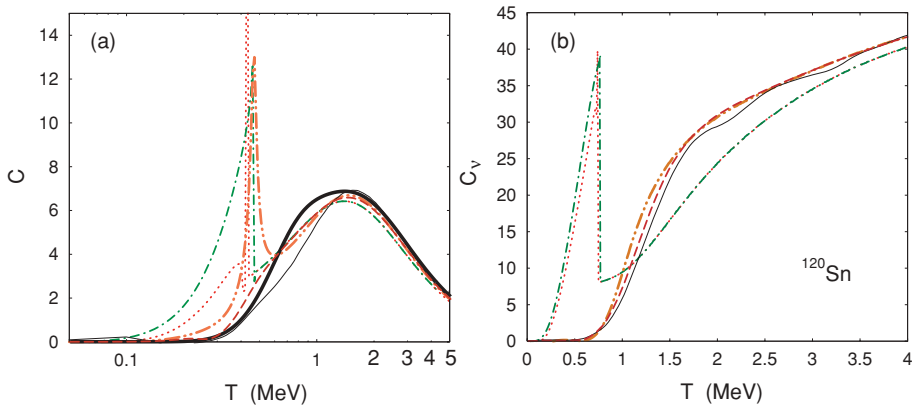

FIG. 5. (Color online) Heat capacities as functions of temperature within the Richardson model for ($\Omega = 11$, $N = 10$) (a) and for neutrons in ^{120}Sn (b). Notations are as in Fig. 2.

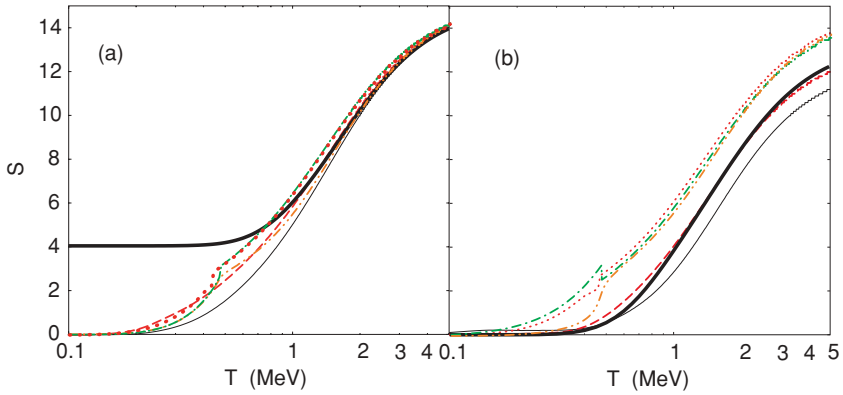

FIG. 6. (Color online) Quasiparticle (single-particle) (a) and thermodynamic (b) entropies as functions of temperature within the Richardson model for ($\Omega = 11$, $N = 10$). Notations are as in Fig. 2. The exact result (thick solid line) in (a) is the single-particle entropy.

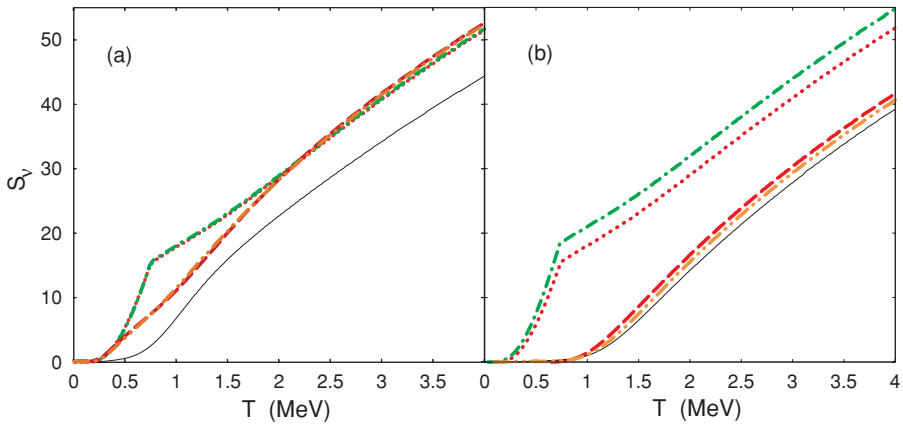

FIG. 7. (Color online) Same as Fig. 6, but for neutron system in ^{120}Sn.

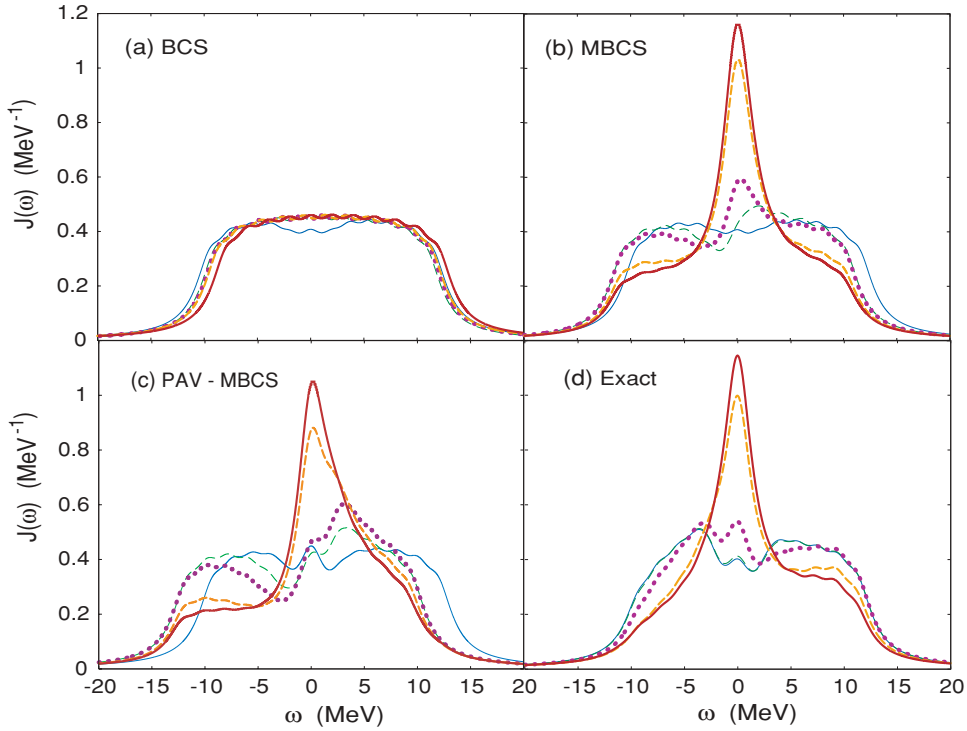

FIG. 8. (Color online) Total pairing spectral function $J(\omega)$ within the Richardson model for ($\Omega = 11$, $N = 10$) as predicted by the BCS (a), MBCS (b), PAV-MBCS (c) theories, and exact solutions (d) at temperatures $T = 0, 0.5, 1, 3$, and 5 MeV as indicated by the thin solid, thin dashed, dotted, thick dashed, and thick solid lines, respectively. The calculations used a half-width $\varepsilon = 0.8$ MeV.

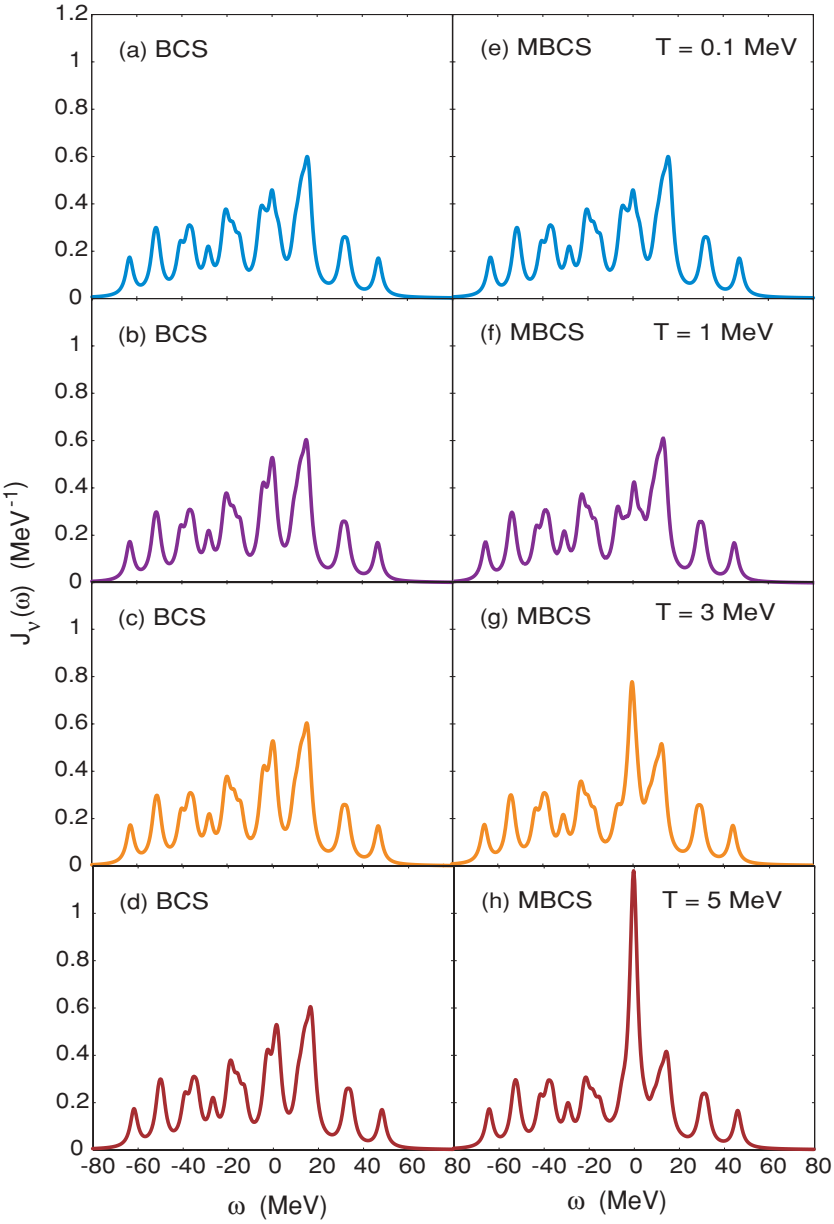

FIG. 9. (Color online) Total pairing spectral function $J_\nu(\omega)$ for neutrons in ^{120}Sn as predicted by the BCS [(a)–(d)] and MBCS [(e)–(h)] theories at $T = 0.1, 1, 3$, and 5 MeV as indicated in the panels. The calculations used a half-width $\varepsilon = 0.8$ MeV.

are different at the edges of the spectrum in such a way that $S_{\rm th} < S_{\rm sp}$. One notices that the predictions for the quasiparticle and single-particle entropies by all approximations coalesce at high T, except for PAV-MBCS $S_{\rm qp}$ for ^{120}Sn, which is substantially lower because of the large difference between the PAV-MBCS gap and the values obtained within the MBCS theory and MLN method. Concerning the thermodynamic entropy, the values for $S_{\rm th}$ obtained within the MLN method as well as the MBCS and PAV-MBCS theories are significantly lower than those predicted within the BCS theory and LN method.

F. Pairing spectral function

The total pairing spectral function $J(\omega)$ of Eq. (33) is calculated at various temperatures and values for the half-width ε of the pairing excitations. The results obtained within the Richardson model with ($\Omega = 11$, $N = 10$, $\varepsilon = 0.8$ MeV) as predicted by the BCS, MBCS, PAV-MBCS theories, as well as the exact results are shown in Fig. 8. The exact results are here defined as those obtained by replacing the coefficients $\bar{v}_j^2$ and $\bar{u}_j^2$ in Eq. (33) with the occupation numbers f_j and $1 - f_j$, respectively, which are given by averaging the exact occupation numbers within the canonical ensemble of N particles at temperature T (see Ref. [17]). At very low T (0.1 MeV), all the results show a clear evidence of superfluid pairing correlations as a depletion of $J(\omega)$ at around $\omega = 0$. Within the BCS theory, this valley becomes shallower as T increases, and it disappears at $T = T_c$; beyond that temperature, the BCS results remain stable relative to T. Meanwhile, the MBCS, PAV-MBCS, and exact results show the spectacular development of a peak at $\omega = 0$, which is

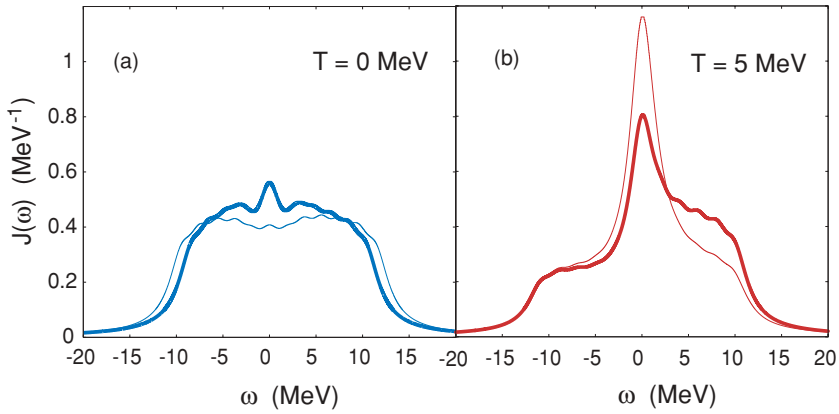

FIG. 10. (Color online) Total pairing spectral function $J(\omega)$ within the Richardson model for for ($\Omega = 11$, $N = 10$) at $T = 0$ (a) and 5 MeV (b) obtained within the MBCS theory (thin lines) and MLN method (thick lines).

growing with T as a clear manifestation of the pseudogap $\delta\Delta$ (11). Using a smaller value ε for the half-width of pairing excitation leads to more splitting, while increasing ε smooths out the fine structure of the distribution. However the enhancement of the peak at $\omega = 0$ remains with increasing T within the MBCS and PAV-MBCS theories as well as the exact solutions. A similar feature is also seen in the total neutron pairing spectral function for ^{120}Sn as shown in Fig. 9. Here, within the BCS theory, except for some very small change in the peak at $\omega = 0$, the whole distribution remains nearly unchanged as T varies. Within the MBCS theory, the peak at $\omega = 0$ grows with T, while the one at $\omega \simeq 15$ MeV becomes depleted as T increases. The PNP with the MLN method does not change the qualitative picture of the growing peak at $\omega = 0$ with T, although it does lower the peak, as can be seen in Fig. 10.

To look into the source of the enhancement of the total pairing spectral function $J(\omega)$ of Eq. (33) at $\omega = 0$ with increasing T, let us examine the components $J_U(\omega)$, $J_V(\omega)$ [Eq. (34)], and $J_{UV}(\omega)$ [Eq. (35)] of the function $J(\omega)$. These functions reach maximum values at $\omega = 2\bar{E}_j$, $-2\bar{E}_j$, and 0, respectively. The temperature dependences of their profiles are also determined by $\bar{u}_j^4$, $\bar{v}_j^4$, and $\bar{u}_j^2\bar{v}_j^2$, respectively. The latter, obtained within the BCS and MBCS theories at several temperatures, are depicted in Fig. 11 as functions of single-particle energies. The cases with the PAV-MBCS theory and exact results are not shown, as they are qualitatively similar to those predicted with the MBCS theory. Within the BCS theory, the coefficients u_j and v_j have the profiles approaching the step functions with increasing T so that $u_j = 1$, $v_j = 0$ at $\epsilon_j - \lambda > 0$, and $u_j = 0$, $v_j = 1$ at $\epsilon_j - \lambda < 0$ when $T \geqslant T_c$. The product $u_j v_j$ decreases with increasing T and vanishes at $T \geqslant T_c$. This leads to a similar evolution of functions u_j^4, v_j^4, and $u_j^2 v_j^2$ with increasing T as shown in Figs. 11(a)–11(c). At the same time, the MBCS functions $\bar{u}_j^4$, $\bar{v}_j^4$, and $\bar{u}_j^2\bar{v}_j^2$ have different temperature dependences due to the presence of $\delta\mathcal{N}_j$,

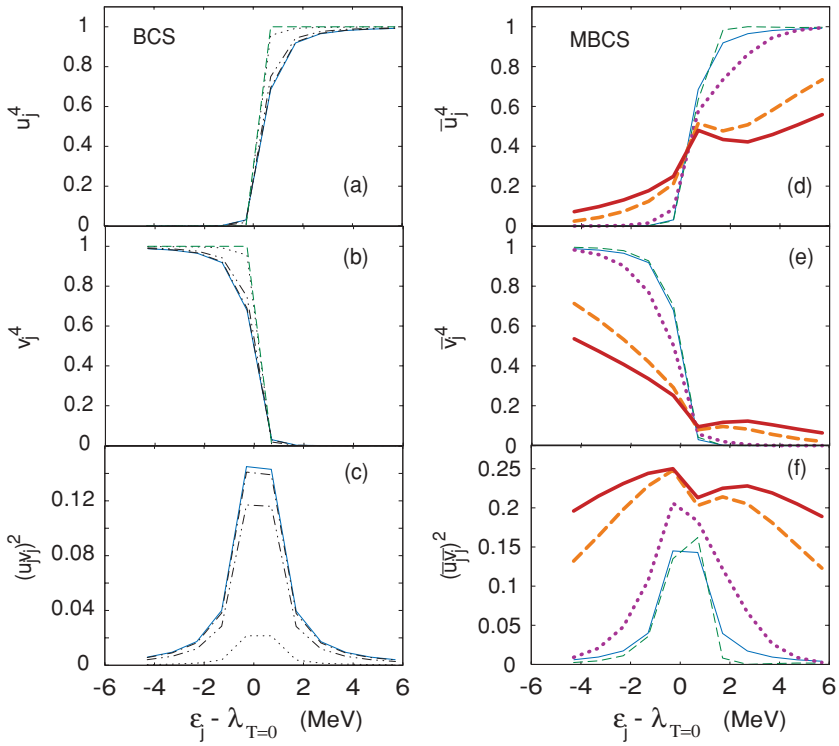

FIG. 11. (Color online) Functions u_j^4, v_j^4, $u_j^2 v_j^2$, $\bar{u}_j^4$, $\bar{v}_j^4$, and $\bar{u}_j^2\bar{v}_j^2$ obtained in the Richardson model with ($\Omega = 11$, $N = 10$) vs $\epsilon_j - \lambda_{T=0}$ at several temperatures. Lines connect discrete points to guide the eye. In (a)–(c) the thin solid, dash-dotted, dash-double-dotted, dotted, and dashed lines denote results obtained with the BCS theory at $T = 0, 0.1, 0.2, 0.3$, and 0.5 MeV, respectively. In (d)–(f), the thin solid, thin dashed, thick dotted, thick dashed, and thick solid lines stand for results obtained within the MBCS theory at $T = 0, 0.5, 1, 3$, and 5 MeV, respectively.

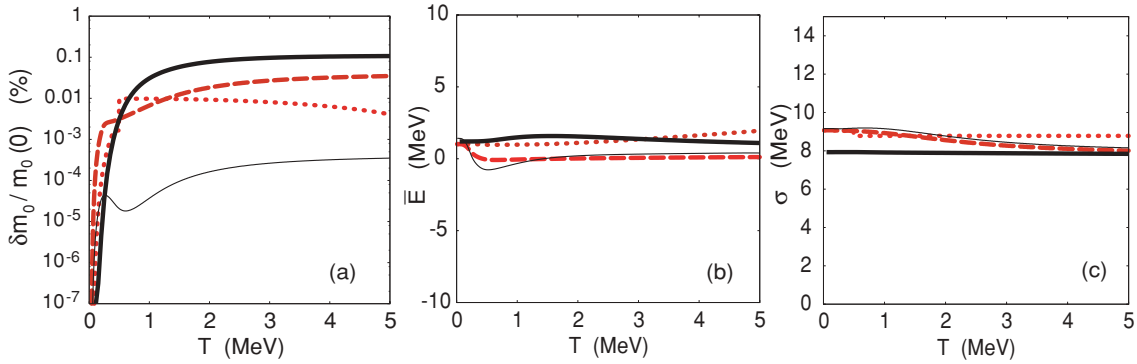

FIG. 12. (Color online) Relative errors for the first moment (a) (see text), centroid energies (b), and spreading widths σ (c) as functions of T obtained within the Richardson model for ($\Omega = 11$, $N = 10$). The notations are as in Fig. 2.

which increases with T as was shown in Figs. 1(a)–1(c) above, as well as in Fig. 1(f) of Ref. [18] and Fig. 2 of Ref. [17]. Functions $\bar{u}_j^4$ and $\bar{v}_j^4$ become depleted, while $\bar{u}_j^2\bar{v}_j^2$ is enhanced as T increases. Since $\bar{u}_j^2\bar{v}_j^2$ are the components of the modified pairing tensor, their enhancement with T is physically related to the existence of the pseudogap induced by the QNF. As a consequence, the components $J_U(\omega)$ and $J_V(\omega)$ within the BCS theory become rather stable against T, while the component $J_{UV}(\omega)$ decreases with increasing T and vanishes at $T \geqslant T_c$. Within the MBCS theory, the temperature dependences of $\bar{u}_j^4$, $\bar{v}_j^4$, and $\bar{u}_j^2\bar{v}_j^2$ cause a depletion of $J_U(\omega)$ and $J_V(\omega)$ with increasing T, while $J_{UV}(\omega)$ gets enhanced dramatically, so that at $T > 2$ MeV, its maximum value at $\omega = 0$ becomes much higher than those of $J_U(\omega)$ and $J_V(\omega)$. This behavior leads to the enhancement of the total pairing spectral function $J(\omega)$ at $\omega = 0$ with increasing T as shown in Fig. 8. The same reasoning holds for the total pairing spectral function $J(\omega)$ for neutrons in the realistic nucleus ^{120}Sn (Fig. 9).

The temperature dependences of integrated quantities of the total pairing spectral function $J(\omega)$ are shown in Fig. 12. All the integrations are carried out from $E_1 = -40$ MeV up to $E_2 = 40$ MeV. The relative errors of the zeroth moments $\delta m_0(T)/m_0(0) \equiv |m_0(T) - m_0(0)|/m_0(0)$ obtained within the BCS, MBCS, and PAV-MBCS theories are compared with the exact values in Fig. 12(a). It is seen that although all the integrated strengths increase with T up to $T \simeq T_c$ and roughly saturate at high T, these changes are extremely small (below 0.1%). This shows that the sum rule is well preserved at finite temperature. The centroid energy, which is obtained as the ratio between the energy-weighted sum and the total sum of strengths, is also rather stable against temperature within all the approximations under consideration, which is in good agreement with the exact result, as shown in Fig. 12(b). Finally, it is found that the spreading width σ predicted by the BCS theory is around 9 MeV, which is higher than the exact value of around 8 MeV. These two values are rather temperature independent, while the predicted values within the MBCS and PAV-MBCS theories for σ decrease from the BCS value to the exact one with increasing T.

IV. CONCLUSIONS

In this paper, particle-number projection (PNP) has been carried out within the MBCS theory by using the Lipkin-Nogami (LN) method and projection after variation (PAV). When applied to the BCS wave functions, the variation after projection (VAP) such as the LN method is usually better than the PAV. However, for the MBCS theory, where the sharp SN phase transition is smoothed out, the calculations carried out within the Richardson model show that the PAV-MBCS theory offers predictions closer to the exact results than those obtained within the MLN method for the pairing gap, energy of the system, and other thermodynamic characteristics such as heat capacity and entropies. The application to a realistic heavy nucleus ^{120}Sn with an open shell for neutrons shows small effects caused by PNP, which do not change the qualitative picture of smoothing out the sharp SN phase transition due to the quasiparticle-number fluctuations (QNF) within the MBCS theory. The results of temperature-dependent total spectral pairing functions reveal a spectacular manifestation of the pseudogap caused by the QNF in the form of a peak at zero energy, which grows with temperature. It is now possible to confirm the reliability of the conclusion that the sharp SN phase transition in finite nuclei at finite temperature is smoothed out, and this is the consequence of the large QNF due to the finiteness of the system, as has been microscopically proved within the MBCS theory in the recent series of papers [15–18].

As a next step in this direction, it will be interesting to study microscopically the effects caused by quantal and thermal fluctuations in hot rotating nuclei. To realize this, the angular-momentum effect needs to be included in the MBCS theory. This study is now underway [27], and the results will be reported in a forthcoming paper.

ACKNOWLEDGEMENT

The calculations were carried out using the RIKEN Super-combined Cluster System with the FORTRAN IMSL Library 3.0 by Visual Numerics.

[1] J. Bardeen, L. Cooper, and J. Schrieffer, Phys. Rev. **108**, 1175 (1957).
[2] L. D. Landau and E. M. Lifshitz, *Course of Theoretical Physics* (Nauka, Moscow, 1964), Vol. 5, pp. 297, 308.
[3] D. N. Zubarev, Sov. Phys. Usp. **3**, 320 (1960).
[4] R. W. Richardson, Phys. Lett. **3**, 277 (1963); **5**, 82 (1963); **14**, 325 (1965).
[5] F. Pan, J. P. Draayer, and W. E. Ormand, Phys. Lett. **B422**, 1 (1998).
[6] A. Volya, B. A. Brown, and V. Zelevinsky, Phys. Lett. **B509**, 37 (2001).
[7] H. J. Lipkin, Ann. Phys. (NY) **9**, 272 (1960); Y. Nogami and I. J. Zucker, Nucl. Phys. **60**, 203 (1964); J. F. Goodfellow and Y. Nogami, Can. J. Phys. **44**, 1321 (1966).
[8] H. C. Pradhan, Y. Nogami, and J. Law, Nucl. Phys. **A201**, 357 (1973).
[9] N. D. Dang, Eur. Phys. J. A **16**, 181 (2003).
[10] N. Q. Hung and N. D. Dang, Phys. Rev. C **76**, 054302 (2007).
[11] L. G. Moretto, Nucl. Phys. **A182**, 641 (1972).
[12] A. L. Goodman, Phys. Rev. C **29**, 1887 (1984).
[13] N. Dinh Dang and N. Zuy Thang, J. Phys. G **14**, 1471 (1988).
[14] N. D. Dang, P. Ring, and R. Rossignoli, Phys. Rev. C **47**, 606 (1993); R. Rossignoli, P. Ring, and N. D. Dang, Phys. Lett. **B297**, 9 (1992).
[15] N. Dinh Dang and V. Zelevinsky, Phys. Rev. C **64**, 064319 (2001).
[16] N. Dinh Dang and A. Arima, Phys. Rev. C **67**, 014304 (2003).
[17] N. Dinh Dang, Nucl. Phys. **A784**, 147 (2007).
[18] N. D. Dang and A. Arima, Phys. Rev. C **68**, 014318 (2003).
[19] V. J. Emery and S. A. Kivelson, Nature (London) **374**, 434 (1995); V. M. Loktev, R. M. Quick, and S. G. Sharapov, Phys. Rep. **349**, 1 (2001).
[20] P. Magierski, S. Cwiok, J. Dobaczewski, and W. Nazarewicz, Phys. Rev. C **48**, 1686 (1993).
[21] A. L. Goodman, Nucl. Phys. **A352**, 30 (1981).
[22] V. Zelevinsky, B. A. Brown, N. Frazier, and M. Horoi, Phys. Rep. **276**, 85 (1996).
[23] V. Yu. Ponomarev and A. I. Vdovin, Phys. Rev. C **72**, 034309 (2005).
[24] N. D. Dang and A. Arima, Phys. Rev. C **74**, 059801 (2006).
[25] V. Yu. Ponomarev and A. I. Vdovin, Phys. Rev. C **74**, 059802 (2006).
[26] P. Bonche, S. Levit, and D. Vautherin, Nucl. Phys. **A427**, 278 (1984).
[27] N. Quang Hung and N. Dinh Dang (in preparation).